H_2 production from partial oxidation of CH_4 by Fe_2O_3-supported Ni-based catalysts in a plasma-assisted packed bed reactor

Yaoyao Zheng[*1], Rob Grant[2], Wenting Hu[3], Ewa Marek[1] and Stuart A. Scott[1]

[1]*Department of Engineering, University of Cambridge, Trumpington Street, Cambridge, CB2 1PZ, United Kingdom.*

[2]*Gas Recovery & Recycle Ltd, Aztec House, Perrywood Business Park, Salfords, Surrey, RH1 5DZ, United Kingdom*

[3]*School of Engineering, Newcastle University, Newcastle upon Tyne, NE1 7RU, United Kingdom*

[*]Corresponding Author: yz450@cam.ac.uk

Abstract

H_2-rich gas production from CH_4 at mild temperature (673 K), was achieved in a single step without introducing a separate oxygen stream. This was conducted in a plasma-assisted packed bed reactor in the presence of Ni-based catalysts doped on an active support, i.e. Fe_2O_3. Among the tested materials, NiO/Fe_2O_3 was found to be very promising and its excellent catalytic properties seemed to be induced by the presence of Fe_2O_3, which suppressed the formation of deposited carbon, and thus maintained the catalytic effect of metallic Ni (formed during NiO reduction by the CH_4/Ar plasma). This work demonstrates the potential of plasma-assisted chemical looping partial oxidation for H_2 production.

Keywords: plasma, chemical looping, H_2 production, catalyst

1. Introduction

Steam reforming of natural gas is used industrially for H_2-rich gas production. The reforming reaction is endothermic and carried out at temperatures above 1073 K [1]. To improve the yield of H_2, water-gas shift (WGS) is usually employed and operated at much lower temperatures (~ 673 K) due to the equilibrium constraints. Overall, the process is endothermic and external heating is needed. The fact that multiple stages are adopted in CH_4-steam reforming makes it more appropriate for large scale processing and applications not requiring high purity H_2.

Chemical looping H_2 production, which employs solid oxygen carriers cycled between two interconnected reactors, has been actively studied due to its potential of achieving high yield and purity of H_2 [2–4]. This technique usually requires high temperatures (~ 1073 K). For small- and medium-scale H_2 production, suitable techniques also include water splitting (e.g. electrolysis) and plasma (particularly non-thermal) -assisted reforming processes [5]. Electrolysis is widely used but its significant electricity demand, high cost of catalysts, and the need to pretreat water, are issues [6]. In processes assisted by non-thermal plasma, H_2 is produced at lower temperatures than would otherwise be possible [7–9]. CO_2 or steam reforming of methane for H_2 production in dielectric barrier discharge (DBD) reactors is one of the most attractive approaches [7]. To achieve a high yield of H_2, the process often includes catalysts and Ni-based catalysts are commonly used due to their low cost and high catalytic activity. This, however, also implies short lifetime, as Ni-catalysts suffer from carbon deposition, and deactivation [10].

Here, a DBD reactor is used to achieve H_2 production from CH_4 at 673 K. In contrast to conventional plasma-assisted systems, an active oxygen carrier, Fe_2O_3, is proposed as the support for Ni-based catalyst. The introduction of Fe_2O_3 aims to provide a source of oxygen to suppress the carbon deposition, so that the activity of Ni could be maintained. The likely advantages of this plasma-assisted chemical looping H_2 production (PCLH) approach are: (i) operating at low temperatures to favour selectivity for H_2 and to reduce any downstream processing; ii) the chemical loop itself allows oxygen to be added to the process without a separate stream of oxygen.

2. Experimental

2.1 Materials

Fe_2O_3-supported Ni-based materials

Two Fe_2O_3-supported catalysts were prepared: NiO/Fe_2O_3 and $NiFe_2O_4/Fe_2O_3$. Pure Fe_2O_3 was also studied for comparison. Fe_2O_3 particles were prepared from iron oxide powders (Fisher Scientific; 10 μm, > 95 wt%) by granulation, using de-ionised (DI) water (1/10th the mass of Fe_2O_3), as a binder. After mixing, the resulting granules were sieved to 600 – 1000 μm, then calcined at 1273 K for 6 hours in air. The sintered particles were re-sieved to 600 – 850 μm. The Ni-based Fe_2O_3-supported materials were then prepared by dry-impregnation. Nickel nitrate hexahydrate (Sigma-Aldrich, $Ni(NO_3)_2{\cdot}6H_2O$, ≥ 98.5 %), was mixed with the Fe_2O_3 particles,

followed by the addition of DI water to just dissolve the nitrate. The resulting mixture was stirred at 313 K for 20 min, followed by drying at 398 K for 12 hours. The dried mixture was then calcined at 823 K for 5 hours to form NiO/Fe_2O_3, or at 1123 K for 5 hours to produce $NiFe_2O_4/ Fe_2O_3$. In both cases, the molar ratio of Ni to the total metal (i.e. Ni + Fe) was about 1: 10.

Al_2O_3-supported Ni-based materials

As a control, materials were also prepared with Al_2O_3 instead of Fe_2O_3. The preparation of Al_2O_3 started with aluminium oxide pellets (Sigma-Aldrich, γ-Al_2O_3, 3 mm). The pellets were crushed to 600 – 850 μm, and then calcined at 1273 K for 6 hours in air. The preparation of NiO/Al_2O_3 followed the same protocol (i.e. dry-impregnation) as that for NiO/Fe_2O_3. The prepared NiO/Al_2O_3 was then divided into two equal portions. One portion was used as prepared, i.e. NiO/Al_2O_3. The other portion was reduced at 1073 K in 5 % H_2 (balance N_2, BOC) for 30 min to obtain Ni/Al_2O_3. Similarly, the resulting Al_2O_3-supported Ni-based particles had a sieve size of 600 – 850 μm, with a Ni to total metal molar ratio of 1: 10.

2.2 Apparatus

The DBD reactor (Fig. 1) was made of a quartz tube (i.d. 25.0 mm, o.d. 28.0 mm), acting as the packed bed reactor as well as the dielectric material between the two electrodes. A co-axial stainless-steel rod (diameter of 12.0 mm) within the quartz tube formed the high voltage electrode. A stainless-steel mesh wrapped around the outer surface of the quartz tube formed the ground electrode, enclosing a height of 20 mm. The gap between the quartz tube and the high voltage rod surface (6.5 mm) was the plasma discharge zone and was packed with the prepared materials (a volume of 7.5 ml). The system was operated at atmospheric pressure and heated externally with its temperature measured by a K-type thermocouple (positioned outside the DBD reactor, the temperature inside the bed was about 5 K higher). AC power (primary) was supplied to the DBD reactor with a voltage of 10.5 $\pm$ 1.0 kV and frequency 26.0 $\pm$ 3.0 kHz (PVM500-2500, Information Unlimited). The dissipated plasma power (determined by Q-V Lissajous plot) was controlled at 7.2 $\pm$ 0.7 W.

The gas stream entered the DBD reactor from the bottom at 0.75 L/min (all the flow rates are expressed at 293 K and 1 atm), low enough to prevent fluidisation. The product gas was sampled at 0.5 L/min. H_2 and O_2 were measured by a thermal conductivity analyser (ABB, Caldos27) and a paramagnetic oxygen analyser (ABB, magnos206), respectively. Carbon-containing gas species were measured by a Fourier transform infrared (FTIR,

MKS Instruments - MultiGas^{TM}) analyser. For a typical experiment, the reactor was heated to 673 K in flowing air (BOC, 99.995%), followed by Ar (BOC, 99.998%) to purge the system before the start of the experiment. During an experiment, a stream of CH_4 (BOC, 99.5%) was mixed with Ar to give 8.5 $\pm$ 0.5 vol% CH_4. After the mixed gas flow stabilised, the plasma was applied. For each experiment, the plasma discharge period was about 5.6 $\pm$ 0.5 min. After CH_4/Ar plasma discharge, the gas was switched to air to burn off any deposited carbon as well as re-oxidise the bed materials. Plasma discharge was later introduced to assist the process of de-coking and re-oxidation. The reduction-oxidation cycle was repeated three times.

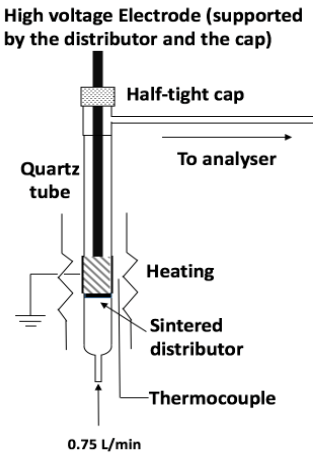

Figure 1 Illustration of the DBD reactor.

2.3 Data analysis

The main gaseous products observed were H_2, CO, CO_2, with traces of C_2H_2, and C_2H_4 (< 150 ppm). The averaged conversion of CH_4, X_{CH_4}, is defined as:

$$X_{CH_4} = \frac{\frac{\int_{t_0}^{t_{end}} (F_{total,0} \cdot x_{CH_4,0} - F_{total} \cdot x_{CH_4}) dt}{t_{end} - t_0}}{F_{total,0} \cdot x_{CH_4,0}},$$

where $x_{CH_4,0}$ and x_{CH_4} are CH_4 mole fractions measured at the reactor inlet and outlet, respectively. $F_{total,0}$ and F_{total} are the corresponding total flow rates. The converted CH_4 was averaged for the period with plasma discharge. Assuming that the amount of Ar did not change over time, only CO, CO_2, H_2, C_2H_2, C_2H_4 and Ar were present at the outlet, then the total flow rate at the outlet (dry basis), F_{total}, can be obtained from the Ar balance:

$$F_{total,0} \cdot \left(1 - x_{CH_{4,0}}\right) = F_{total} \cdot (1 - x_{CH_4} - x_{CO} - x_{CO_2} - x_{C_2H_2} - x_{C_2H_4}).$$

The averaged selectivities, $S_{a=CO\ or\ CO_2}$ for CO or CO_2, and S_{H_2} for H_2, are given as:

$$S_a = \frac{\int_{t_0}^{t_{end}} F_{total} \cdot x_a dt}{\int_{t_0}^{t_{end}} (F_{total,0} \cdot x_{CH_4,0} - F_{total} \cdot x_{CH_4}) dt}$$

$$S_{H_2} = \frac{\int_{t_0}^{t_{end}} F_{total} \cdot x_{H_2}\, dt}{2 \int_{t_0}^{t_{end}} (F_{total,0} \cdot x_{CH_4,0} - F_{total} \cdot x_{CH_4}) dt},$$

where S_a is based on C in CH_4, and S_{H_2} is based on H in CH_4.

The average yield for each product, Y_i, was defined as the amount of component *i* produced for every mole of CH_4 introduced into the DBD reactor:

$$Y_i = \frac{\frac{\int_{t_0}^{t_{end}} F_{total} \cdot x_i \, dt}{t_{end} - t_0}}{F_{total,0} \cdot x_{CH_4,0}}.$$

The fraction of carbon deposited was estimated from the difference between the carbon input and that detected at the outlet during the reduction period:

$$d_c = 1 - \frac{\int_{t_0}^{t_{end}} F_{total} \cdot (x_{co} + x_{co_2} + 2x_{C_2H_4} + 2x_{C_2H_2}) \, dt}{\int_{t_0}^{t_{end}} (F_{total,0} \cdot x_{CH_4,0} - F_{total} \cdot x_{CH_4}) dt}.$$

The carbon and hydrogen balances were also estimated, and defined as the ratio of carbon/hydrogen-containing species measured to the carbon/hydrogen in the converted CH_4 in a complete looping cycle (i.e. CH_4/Ar plasma discharge followed by air plasma discharge stage).

3. Results

3.1 Al_2O_3 and Fe_2O_3

The results of plasma-assisted cracking or/and partial oxidation of CH_4 in undoped Al_2O_3 and Fe_2O_3 beds are presented in Fig. 2. For both materials, CH_4 conversion was only observed when plasma discharge was applied. H_2 was found to be the main product and its generation over the discharge was relatively uniform. CO and CO_2 were observed only at trace levels (< 250 ppm). This suggests that H_2 was primarily generated from CH_4 cracking by the plasma, and the carbon from the converted CH_4 deposited onto the solid phase. This agrees with the fact that the ratio of generated H_2 to converted CH_4 was 1.7 ± 0.1 (based on three cycles) for both materials. Taking into account C_2H_2 and C_2H_4 generated during discharge period (at ppm levels), over 80 % hydrogen balance was obtained for both materials

(see Table 1). The conversion of CH_4, as well as the generation of H_2, in the Al_2O_3 and Fe_2O_3 beds were similar, suggesting that neither material is a good catalyst for CH_4 cracking. In the air plasma discharge period, trace levels (< 100 ppm) of CO and CO_2 were observed, suggesting the presence of deposited carbon from the cracking process in the bed. However, the deposited carbon could not be removed completely at such low temperatures, even with the assistance of plasma. Further regeneration of the bed was carried out by raising the temperature of the reactor to 823 K for over 30 min until no CO and CO_2 were detected.

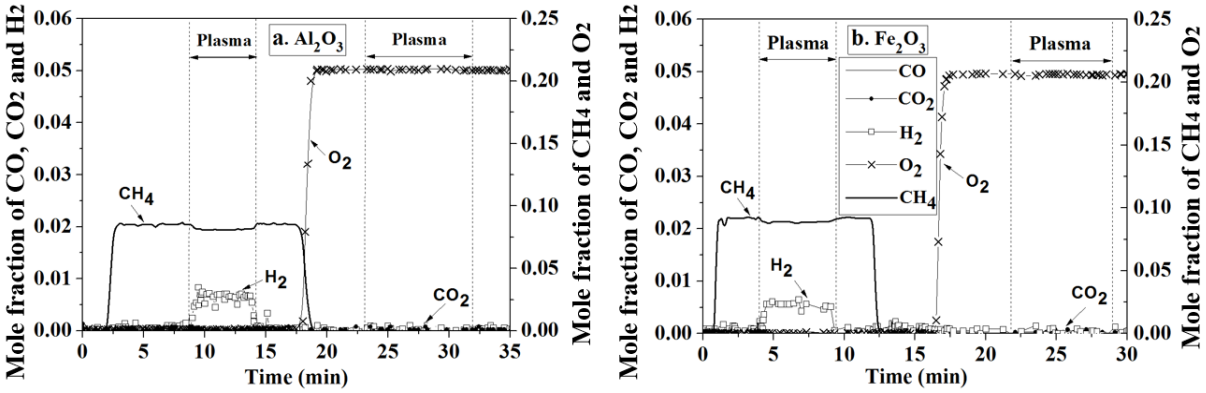

Figure 2 Plasma-assisted cracking/partial oxidation of CH_4 at 673 K with DBD reactor packed with a) Al_2O_3; b) Fe_2O_3.

3.2 NiO/Al_2O_3, Ni/Al_2O_3, NiO/Fe_2O_3 and $NiFe_2O_4/Fe_2O_3$

CH_4 conversion in the NiO/Al_2O_3 bed, shown in Fig. 3a, was similar to those in Al_2O_3 and Fe_2O_3 beds, suggesting that this material also has little effect on CH_4 reforming or partial oxidation. For Ni/Al_2O_3 as seen in Fig. 3b, a significant rise in [H_2] was observed when CH_4 was introduced into the reactor, without plasma. This was mainly due to the catalytic effect of Ni, as reported in e.g. ref [10]. However, the catalytic effect did not last long and the H_2 level dropped and gradually reached a mole fraction of 0.01, whilst no significant production of CO and CO_2 was observed. This suggests that the deactivation of Ni was likely due to carbon deposition. The formation of nickel aluminate (confirmed by post-reaction XRD results shown in Fig. S1) could have also contributed to this deactivation. When plasma discharge was applied from t = 9.5 to t = 15.6 min, higher degrees of CH_4 conversion and H_2 production were achieved. At t = 22.0 min, CH_4 was stopped, leaving the bed purging in Ar. Then, as soon as the

gas was switched from Ar to air, a significant CO_2 peak together with a small CO peak was observed and an overall carbon balance of 94% was obtained.

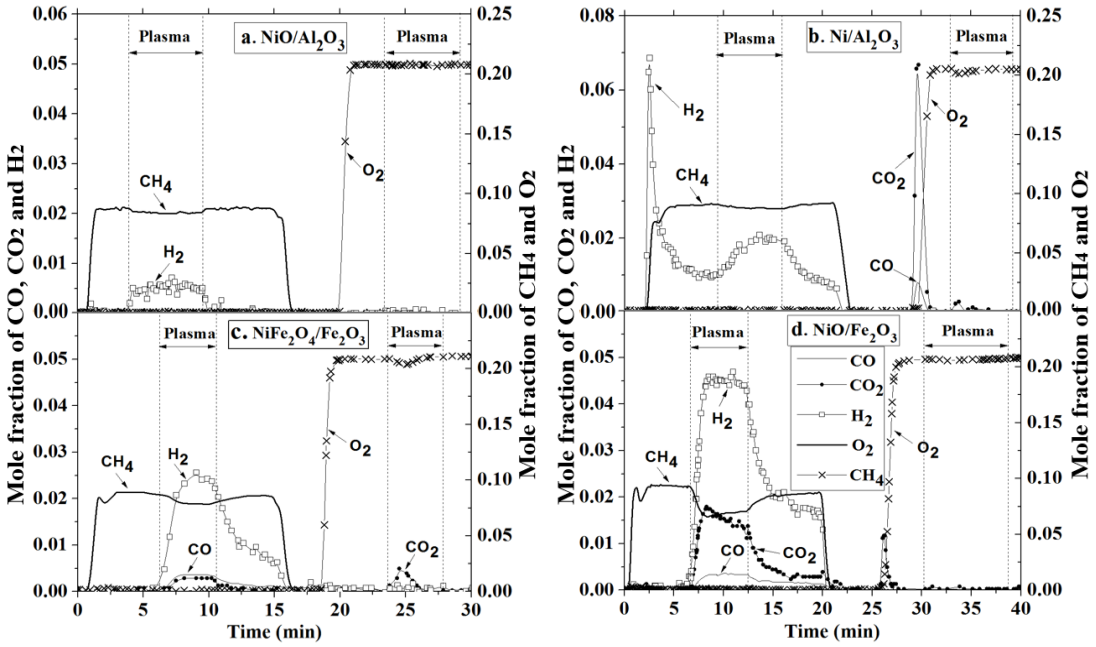

Figure 3 Plasma-assisted cracking/partial oxidation of CH_4 at 673 K with DBD reactor packed with a) NiO/Al_2O_3; b) Ni/Al_2O_3; c) $NiFe_2O_4/Fe_2O_3$; d) NiO/Fe_2O_3.

When the reactor was loaded with $NiFe_2O_4/Fe_2O_3$, according to Fig. 3c, no significant conversion of CH_4 was seen without plasma discharge. At t = 6.8 min, when plasma was introduced, much improved generation of H_2 over the whole discharge period was observed; at the same time, there was a clear production of CO and CO_2, indicating that the reduction of the bed material occurred ($NiFe_2O_4/Fe_2O_3$ was the only source of oxygen in the system). The overall result was a partial oxidation of CH_4 by plasma discharge to a product stream rich in H_2, CO and CO_2. When plasma discharge was stopped, H_2 was still produced from the $NiFe_2O_4/Fe_2O_3$ bed, though at lower levels. The fact that $NiFe_2O_4$ was not reactive for H_2 production before plasma discharge but was after, suggests the generation of some additional phase other than $NiFe_2O_4$ during plasma discharge, with this (probably reduced) phase having a catalytic effect even without plasma. In the air regeneration stage, CO_2 was only observed when

plasma was applied. In the NiO/Fe_2O_3 bed, according to Fig. 3d, no conversion of CH_4 was observed until plasma was applied, at which point a significant amount of H_2 was generated. The CO and CO_2 productions were also much higher than those from other beds during plasma discharge. CH_4 conversion reached 32% in this instance. Similar to the case in the $NiFe_2O_4/Fe_2O_3$ bed, when plasma was switched off, there was still post-plasma H_2 production. Most of the deposited carbon was recovered in air, without the presence of plasma. It should be noted that it was not possible to prepare and investigate Ni/Fe_2O_3 because Ni/Fe_2O_3 is thermodynamically unstable at the studied conditions.

Table 1 Summarised results in different bed materials (errors show the range of three repeats).

Parameters	**Al_2O_3**	**NiO/Al_2O_3**	**Ni/Al_2O_3**	**Fe_2O_3**	**NiO/Fe_2O_3**	**$NiFe_2O_4$/ Fe_2O_3**
d_c	0.75 ± 0.04	0.75 ± 0.03	0.90 ± 0.07	0.71 ± 0.05	0.15 ± 0.03	0.47± 0.08
C balance	0.26 ± 0.02	0.25 ± 0.02	0.94 ± 0.02	0.38 ± 0.02	0.94 ± 0.03	0.63 ± 0.04
H balance	0.93 ± 0.04	0.94 ± 0.03	0.96 ± 0.04	0.82 ± 0.02	0.82 ± 0.03	0.99 ± 0.06
X_{CH_4}	0.05 ± 0.01	0.05 ± 0.01	0.10 ± 0.02	0.04 ± 0.01	0.39 ± 0.07	0.19 ± 0.04
S_{co}	0.01 ± 0.01	0.01 ± 0.01	0.03 ± 0.01	0.01 ± 0.01	0.12 ± 0.01	0.25 ± 0.01
S_{co_2}	0.03 ± 0.01	0.06 ± 0.01	0.02 ± 0.01	0.08 ± 0.01	0.71 ± 0.02	0.27 ± 0.02
S_{H_2}	0.84 ± 0.01	0.85 ± 0.01	0.95 ± 0.01	0.74 ± 0.01	0.92 ± 0.01	0.98 ± 0.07
$Y_{co}\times10^3$	0. 3 ± 0. 1	0.3 ± 0.1	0.3 ± 0.1	0.2 ± 0.1	45.2 ± 4.9	38.4 ± 5.2
$Y_{co_2}\times10^3$	1.2 ± 0.3	2.7 ± 0.5	2.2 ± 0.6	3.2 ± 0.7	285.5 ± 15.1	45.4 ± 3.1
$Y_{H_2}\times10^3$	64.7 ± 1.4	81.3 ± 1.2	180.6 ± 11.2	58.9 ± 1.1	621.7 ± 32.3	319.0 ± 40.2

Table 1 presents the summarised results of degree of carbon deposition, conversion of CH_4, selectivity and yield for products, carbon and hydrogen balances. It should be noted that after three cycles, no mechanical deterioration was visually observed for any of the tested materials. Overall, NiO/Fe_2O_3 seems to be the most promising material for H_2 production due to its low degree of carbon deposition, high carbon and hydrogen balances, and high selectivity and yield for H_2. The hydrogen balance in the case of NiO/Fe_2O_3 was slightly lower than those in other Ni-doped materials. This suggests that some H-containing products other than H_2 might have been generated, probably H_2O. $NiFe_2O_4/Fe_2O_3$ also exhibited very high selectivity towards the production of H_2, although its resistance to coking, carbon balance and the conversion of CH_4 were not as good as those of NiO/Fe_2O_3.

3.3 XRD results for NiO/Fe_2O_3 and $NiFe_2O_4/Fe_2O_3$

To evaluate any possible change in the material structure after the plasma-assisted CH_4 conversion, the bed material samples were collected and X-ray powder diffraction (XRD) performed using an Empyrean PANalytical diffractometer. A typical diffractogram was collected in the range of 2θ from 5° to 80° using Cu K_α radiation with a voltage of 40 kV and current of 40 mA. The phases in the samples were identified using the reference patterns from ICSD database (Table S1).

3.3.1 NiO/Fe_2O_3

Figure 4 shows the XRD patterns of NiO/Fe_2O_3 samples: freshly prepared, with CH_4/Ar plasma treatment and after regeneration in air plasma. Major peaks of each phase and an unknown peak (2θ = 26.7) are marked accordingly. For the freshly calcined NiO/Fe_2O_3, only NiO and Fe_2O_3 were detected. This suggests no chemical interaction between NiO and Fe_2O_3 during calcination. After CH_4/Ar plasma treatment, NiO was no longer detected; instead, metallic Ni and magnetite, Fe_3O_4, were detected. For the air regenerated NiO/Fe_2O_3, similar to the fresh sample, NiO and Fe_2O_3 were the only phases detected, suggesting that the NiO phase can remain separate during plasma discharge in air.

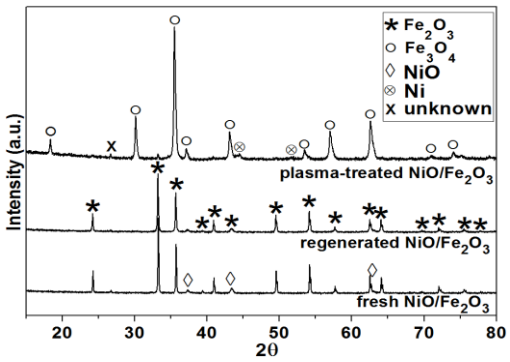

Figure 4 XRD spectra of fresh NiO/Fe_2O_3, CH_4/Ar plasma treated NiO/Fe_2O_3 and air plasma regenerated NiO/Fe_2O_3.

3.3.2 $NiFe_2O_4/Fe_2O_3$

XRD Results for $NiFe_2O_4/Fe_2O_3$ samples are presented in Fig. 5. Fe_2O_3 and $NiFe_2O_4$ phases were observed in the fresh sample. The formation of $NiFe_2O_4$ indicates the diffusion of NiO into the Fe_2O_3 crystal structure during calcination. In the XRD pattern of the CH_4/Ar plasma treated $NiFe_2O_4/Fe_2O_3$,

there was a decrease in the intensity of the peaks for the $NiFe_2O_4$ phase; additionally, metallic alloy of Ni-Fe, expresses as (Ni, Fe), was observed. There was no clear evidence of the presence of Fe_3O_4, suggesting that the oxygen in the produced CO and CO_2 in the CH_4/Ar discharge period probably came from the reduction of $NiFe_2O_4$ to the metallic (Ni, Fe). On regeneration with air, the (Ni, Fe) phase disappeared, but the intensity of $NiFe_2O_4$ peaks did not return to the higher level as seen in the fresh $NiFe_2O_4/Fe_2O_3$ sample.

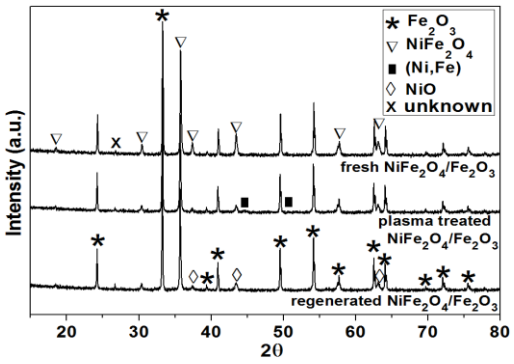

Figure 5 XRD spectra of fresh $NiFe_2O_4/Fe_2O_3$, CH_4/Ar plasma treated $NiFe_2O_4/Fe_2O_3$ and air plasma regenerated $NiFe_2O_4/Fe_2O_3$.

1

2

4. Discussion

4.1 Catalytic activity

The results in Figs. 2 and 3 show that NiO (when supported on inert Al_2O_3) and Fe_2O_3 alone did not show good catalytic activity for the conversion of CH_4, even in the presence of the plasma discharge. However, the combination of NiO and Fe_2O_3, which resulted in NiO/Fe_2O_3 or $NiFe_2O_4/Fe_2O_3$, demonstrated significantly improved performance.

4.1.1 NiO/Fe_2O_3

The results in Fig. 4 imply the formation of Ni when NiO/Fe_2O_3 was subjected to CH_4/Ar plasma discharge. In contrast to the Ni/Al_2O_3 experiment (in Fig. 3b), where the production of H_2 was high at the very beginning of the plasma discharge but decreased quickly, the bed of NiO/Fe_2O_3 was able to

produce significant amounts of H_2 over the entire plasma discharge period. The superior performance of NiO/Fe_2O_3 might have resulted from lattice oxygen in NiO/Fe_2O_3, which seems to suppress the coking of the solid bed, so that the catalytic activity of Ni can be maintained. This is supported by the smaller amount of carbon deposited in the NiO/Fe_2O_3 bed. Owing to the presence of Fe_3O_4, it was difficult to determine if NiO was still present in the plasma treated NiO/Fe_2O_3 sample from the XRD (NiO peaks overlap with those from Fe_3O_4). However, calculation of the oxygen balance can provide additional insight on to the phases present. It was found that the amount of oxygen in the produced CO, CO_2 and H_2O (estimated from the hydrogen balance) during CH_4/Ar plasma discharge period accounted for 3.2 wt% $\pm$ 0.2 wt% of the total mass of NiO/Fe_2O_3. The oxygen capacity from NiO → Ni was 2.0 wt%, whilst that in $Fe_2O_3 \rightarrow Fe_3O_4$ was 3.0 wt%. As most of the hematite was reduced (only low intensity of Fe_2O_3 peaks were detected), it is possible that some NiO might have remained after CH_4/Ar plasma discharge.

Interestingly, the $NiFe_2O_4$ phase was not observed in the XRD pattern of the NiO/Fe_2O_3 (Fig. 4), suggesting little interaction between NiO and Fe_2O_3, either during calcination or plasma treatment. The fact that NiO alone was inactive during plasma discharge, suggests the presence of some available oxygen in the NiO/Fe_2O_3 to suppress coking. One of the three hypothesis might describe these conditions: 1) NiO itself is responsible for the partial oxidation of CH_4 *via* $NiO + CH_4 \rightarrow CO + CO_2 + H_2 + Ni$, and Fe_2O_3 helps the process to continue by transporting oxygen to the Ni sites; 2) metallic Ni is responsible for the generation of H_2 *via* $CH_4 \xrightarrow{Ni} C + H_2$, and the presence of Fe_2O_3 helps to remove the solid carbon from the Ni sites; 3) a combination of 1) and 2). The above results seem to suggest that 2) is more likely to dominate, as the H_2 production rate in the NiO/Fe_2O_3 bed was comparable to that when Ni/Al_2O_3 was just exposed to CH_4. This is further supported by the results from SEM-EDX analysis, which showed that the surface of NiO/Fe_2O_3 particles treated with CH_4/Ar plasma was predominantly covered by Ni (see Fig. S2 and Table S2). Furthermore, the trace amounts of CO and CO_2 produced from NiO/Al_2O_3 subjected to CH_4/Ar plasma discharge were similar to those from bare Al_2O_3 and Fe_2O_3 beds, showing that NiO in the absence of Fe_2O_3 cokes easily, or does not react with CH_4.

It is reasonable to identify the sequence of phase transformation of NiO/Fe_2O_3 in the reducing CH_4 environment by referring to the Ni-O and Fe-O phase diagrams (computed by MTDATA [11], see Figs. S3 and S4). Thermodynamically, at 673 K, the P_{O_2} to cause a phase transition from NiO to Ni is lower than that for Fe_2O_3 to Fe_3O_4, but higher than that for Fe_3O_4 to Fe. This means that assuming negligible solubility of NiO into the Fe_2O_3 system, the sequence for reduction would be: $Fe_2O_3 + NiO \rightarrow NiO + Fe_3O_4 \rightarrow Ni + Fe_3O_4$. Therefore, in a reducing environment, it is expected that if Ni was detected, Fe_3O_4 would then also be present. However, at the relatively mild temperatures in this study, reaction kinetics are important and Fe_2O_3 is un-reactive towards CH_4. A high level of H_2 production in NiO/Fe_2O_3 was observed as soon as the plasma discharge was applied. If the catalytic effect for H_2 production was only due to the presence of metallic Ni, then the formation of Ni must have happened as soon as NiO/Fe_2O_3 was subjected to plasma discharge. This contrasts with the pure NiO/Al_2O_3 material, which could also have reduced to Ni locally, but for some reason remained inactive, perhaps because of coking, with carbon immediately deposited on any newly created Ni-metallic site. Additionally, the formation of nickel aluminate after plasma treatment also means that less Ni was available for CH_4 cracking. If Ni formed immediately when plasma was applied in the NiO/Fe_2O_3 bed, the suppression of coking was most likely due to the presence of an oxygen source, i.e. Fe_2O_3. The co-existence of Ni and Fe_2O_3 is thermodynamically unstable, and the system tends to form NiO and Fe_3O_4 at equilibrium. The transfer of oxygen to the Ni sites would then help remove any deposited carbon, or prevent transiently formed absorbed carbon species from forming coke, and thus maintaining the catalytic activity of Ni. This means that a synergistic effect, which here most likely depends on the CH_4, Ni and oxygen from Fe_2O_3 being in intimate contact, exists. For NiO/Fe_2O_3, not only was less coke formed, but also the remaining coke was more easily burned off during the air regeneration stage, compared with other materials e.g. NiO/Al_2O_3 and Fe_2O_3. The superior performance of the NiO/Fe_2O_3 for H_2 production and its easy regeneration demonstrate the possibility of plasma-assisted chemical looping system for H_2 production at mild temperatures. The process requires further studies and careful optimisation. Interestingly, at higher temperatures, as observed in preliminary tests at 773 K, plasma treatment on NiO/Fe_2O_3 resulted in total combustion of CH_4 to H_2O and CO_2.

4.1.2 $NiFe_2O_4/Fe_2O_3$

As shown in Fig. 4, the observed (Ni, Fe) phase together with the decreased intensity of $NiFe_2O_4$ peaks in the XRD spectra in the CH_4/Ar plasma treated sample, indicates the phase segregation of $NiFe_2O_4$ to (Ni,Fe). This seems to be consistent with the study carried out by Raghavan [12]. At 1273 K and low P_{O_2} (P_{O_2} < 10^{-11} bar)**,** $NiFe_2O_4$ tends to reach equilibrium with $(Ni, Fe)_3O_4$ and (Ni, Fe). Extrapolating to the low temperatures used here, it is reasonable to expect that the reduction follows $NiFe_2O_4 \rightarrow (Ni, Fe)_3O_4$ + (Ni, Fe). In our study, when the $NiFe_2O_4$ material was regenerated in air plasma at 673 K (Fig. 5), the (Ni, Fe) peaks disappeared. The most likely route for Ni oxidation is to create NiO. However, the presence of NiO was difficult to confirm, due to significant overlap of the NiO and $NiFe_2O_4$ peaks in the XRD pattern. For Fe, no evidence of wustite or magnetite phase was observed, and the most likely route would then be $Fe \rightarrow Fe_2O_3$. In terms of the catalytic effect in the $NiFe_2O_4$ bed, it was found that H_2 yield improved slightly in the second and third reduction cycles (Fig. S5). If NiO was indeed created in the regeneration stage, then it could have helped with the production of H_2 in subsequent reductions.

4.2 Comparison to water gas shift equilibrium

In NiO/Fe_2O_3, the products from CH_4/Ar plasma discharge were mainly H_2 and CO_2. A high yield of H_2 and CO_2 at such low temperature (673 K) could be linked with WGS ($H_2O + CO \rightarrow H_2 + CO_2$). Assuming that water was also produced and is responsible for the missing H in the mass balance (as shown in Table 1), then the reaction quotient, $\frac{[H_2][CO_2]}{[H_2O][CO]}$= 64.6 $\pm$ 19.1, can be compared with the equilibrium constant of WGS at 673 K, K_{eq} = 12.0 [13]. This suggests that the plasma-assisted process tends to push production of H_2 and CO_2, beyond the thermodynamic equilibrium of WGS. To achieve a K_{eq} close to the reaction quotient obtained here, the conventional WGS would need to operate at a lower temperature (though it should be noted that excess water is usually used to shift the equilibrium). For the WGS to achieve a high conversion to H_2 and maintain favourable kinetics, multiple reaction stages are often employed (e.g. moving from high to low temperatures), and thus complicating the process. For the presented PCLH approach, the fact that such high production of H_2 and CO_2 was

achieved within such a small bed (~ 7.5 ml) indicates fast reaction rates. The high value of $\frac{[H_2][CO_2]}{[H_2O][CO]}$ found here seems to suggest that H_2 and CO_2 might be directly produced from the partial oxidation of CH_4 by the oxygen carrier, without going through some intermediate steps involving WGS. The unusually high ratio is likely to be a result of H_2 and CO_2 not having sufficient time to reach a WGS equilibrium.

4.3 Energy cost for H_2 production

Assuming electricity production from CH_4 combustion with 60% efficiency (see supplementary information Eq. S1), the estimated energy cost for H_2 production from a NiO/Fe_2O_3 bed, is 440 ± 20 MJ/kg of produced H_2 (based on HHV of CH_4). This is higher than the cost of conventional steam methane reforming, which is less than 160 MJ/kg [14], but comparable to that of water electrolysis, from 320 to 510 MJ/kg (estimated based on electricity consumption between 50 to 79 kWh/kg [15]). Given that the current experimental set-up can be further optimised, there is scope for further cost reduction.

5. Conclusions

Ni-based catalysts supported on Al_2O_3 and Fe_2O_3 were investigated for plasma-assisted H_2 production from CH_4. Experiments carried out in a DBD packed bed reactor at 673 K showed that the supporting metal oxide, Fe_2O_3, positively influences the activity of the catalyst. Among the tested materials, NiO/Fe_2O_3 exhibited the highest H_2 yield, whilst carbon deposition and the subsequent catalyst deactivation were significantly lower than those from NiO or Ni supported on alumina.

The catalytic activity for H_2 production in the combined catalyst/oxygen carrier (NiO/Fe_2O_3) was attributed to the generation of metallic Ni, and the suppression of carbon deposition was connected to the presence of the active metal oxide, Fe_2O_3. The hydrogen yield form the plasma-assisted CH_4 reforming and oxidation by the oxygen carrier exceeded that anticipated from the WGS equilibrium.

6. Acknowledgements

Yaoyao Zheng is grateful for the financial support from the China Scholarship Council and Cambridge Trust.

7. References

[1] J.R. Rostrup-Nielsen, T. Rostrup-Nielsen, CATTECH 6 (2002) 150–159.

[2] M. Rydén, A. Lyngfelt, Int. J. Hydrogen Energy 31 (2006) 1271–1283.

[3] M. Tang, L. Xu, M. Fan, Appl. Energy 151 (2015) 143–156.

[4] J. Adanez, A. Abad, F. Garcia-Labiano, P. Gayan, L.F. de Diego, Prog. Energy Combust. Sci. 38 (2012) 215–282.

[5] N.Z. Muradov, T.N. Veziroğlu, Int. J. Hydrogen Energy 30 (2005) 225–237.

[6] J. Genovese, K. Harg, M. Paster, J. Turner, Analysis (2009) 51.

[7] Q. Wang, H. Shi, B. Yan, Y. Jin, Y. Cheng, Int. J. Hydrogen Energy 36 (2011) 8301–8306.

[8] H. Taghvaei, M.M. Shirazi, N. Hooshmand, M.R. Rahimpour, A. Jahanmiri, Appl. Energy 98 (2012) 3–10.

[9] Y.X. Zeng, L. Wang, C.F. Wu, J.Q. Wang, B.X. Shen, X. Tu, Appl. Catal. B Environ. 224 (2018) 469–478.

[10] Y.-G. Chen, J. Ren, Catal. Letters 29 (1994) 39–48.

[11] R.H. Davies, A.T. Dinsdale, J.A. Gisby, J.A.J. Robinson, S.M. Martin, Calphad 26 (2002) 229–71.

[12] V. Raghavan, J. Phase Equilibria Diffus. 31 (2010) 369–371.

[13] C.A. Callaghan, Kinetics and Catalysis of the Water-Gas-Shift Reaction: A Microkinetic and

Graph Theoretic Approach, 2006.

[14] P.L. Spath, M.K. Mann, Natl. Renew. Energy Lab. DOE, U.S. (2001) NREL/TP-570-27637.

[15] B. Kruse, S. Grinna, C. Buch, Hydrogen: Status and Possibilities, 2002.

List of supplemental materials

Fig. S1 XRD spectra of CH_4/Ar plasma treated NiO/γ-Al_2O_3. Material was only reduced and not regenerated with air after the plasma treatment.

Fig. S2 SEM micrograph combined with EDX analysis of NiO/Fe_2O_3 particle surface after experiment in the DBD reactor. The material was retreated after CH_4/Ar plasma-assisted reduction (no air regeneration). The micrograph was collected with TESCAN MIRA3 FEG-SEM combined with Oxford Instruments Aztec Energy X-maxN 80 EDS system at an accelerating voltage of 15 kV, working distance of 14 mm and 1000x magnification. The quantitative results from the EDX analysis are presented in Table S2.

Fig. S3 Phase diagram of Ni-O system, calculated with MTDATA [11] (SGTE database).

Fig. S4 Phase diagram of Fe-O system with MTDATA [11] (NPL database).

Fig. S5 H_2 concentration measured during three subsequent CH_4/Ar plasma discharge experiments, using $NiFe_2O_4$/Fe_2O_3 as the bed material.

Table S1 Collection Code of the XRD reference patterns used from ICSD database.

Table S2 Results from the EDX analysis of NiO/Fe_2O_3 particle surface after experiment in the DBD reactor. The material was retreated after CH_4/Ar plasma-assisted reduction (no air regeneration). The analysis was performed with TESCAN MIRA3 FEG-SEM combined with Oxford Instruments Aztec Energy X-maxN 80 EDS system at an accelerating voltage of 15 kV, working distance of 14 mm and 1000x magnification. The SEM micrograph and EDX maps are presented in Fig. S2.

Eq. S1 The energy cost for H_2 production, MJ /kg.

Fig. S1

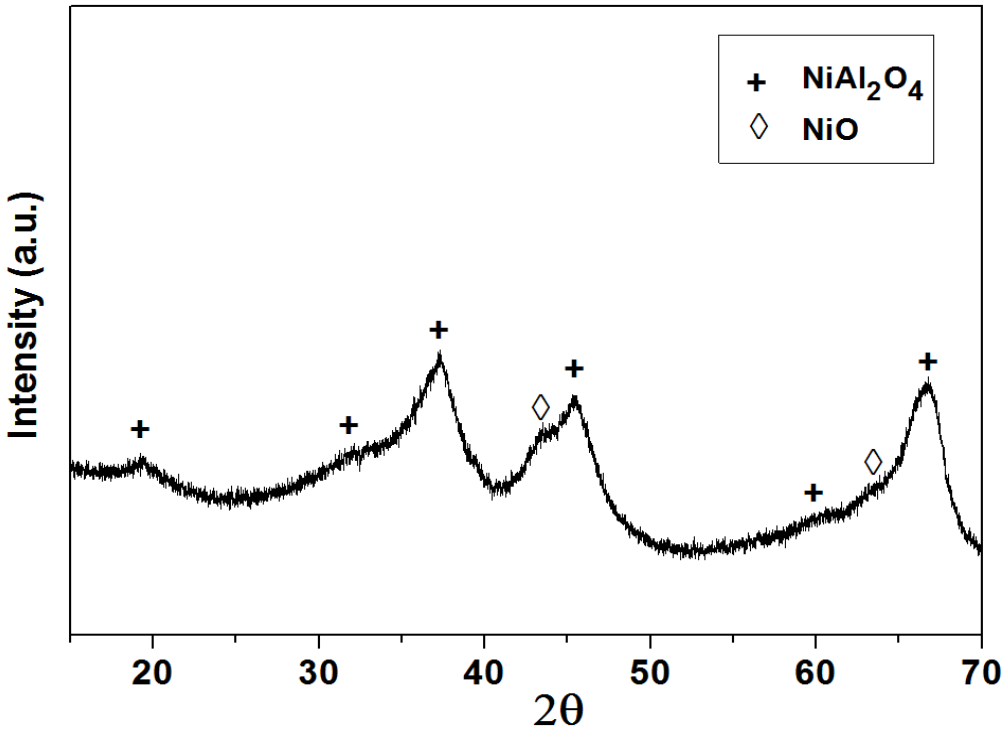

Fig. S2

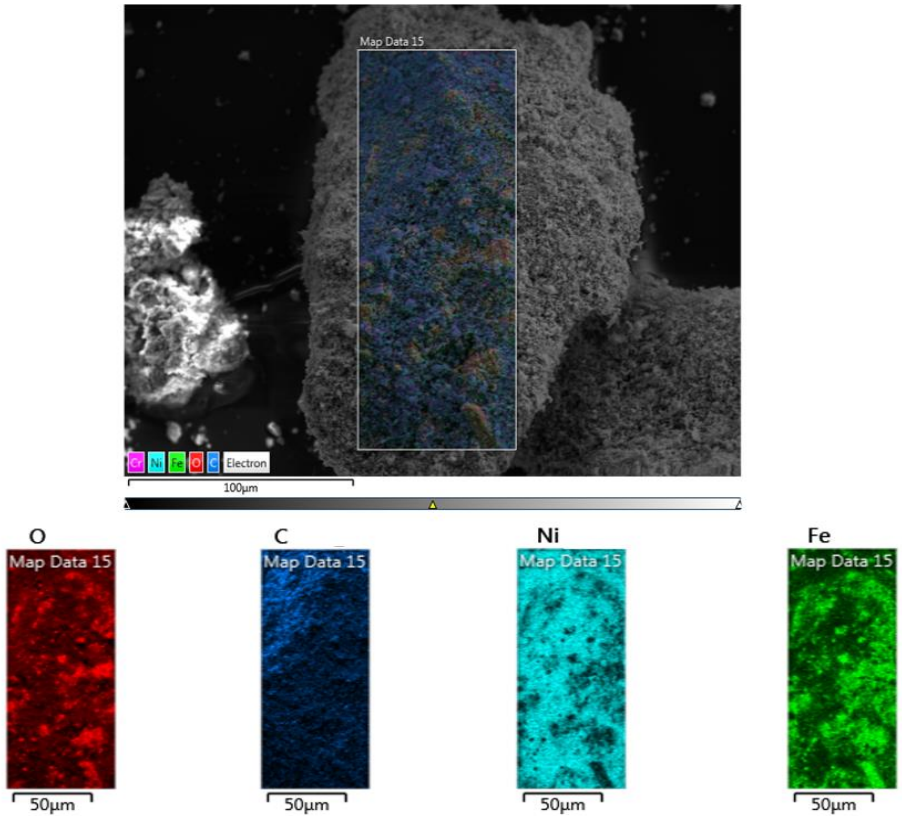
Map Data 15
Cr Ni Fe O C Electron
100µm
O
Map Data 15
50µm
C
Map Data 15
50µm
Ni
Map Data 15
50µm
Fe
Map Data 15
50µm

Fig. S3

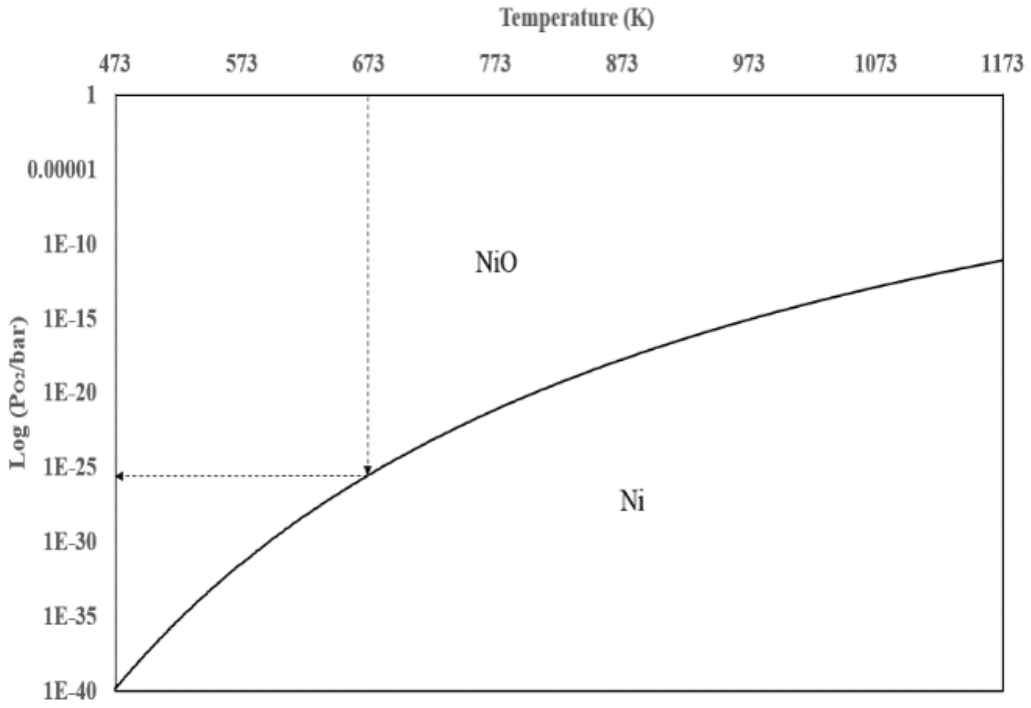
Temperature (K)
473
573
673
773
873
973
1073
1173
1
0.00001
1E-10
1E-15
1E-20
1E-25
1E-30
1E-35
1E-40
Log (Po2/bar)
NiO
Ni

Fig. S4

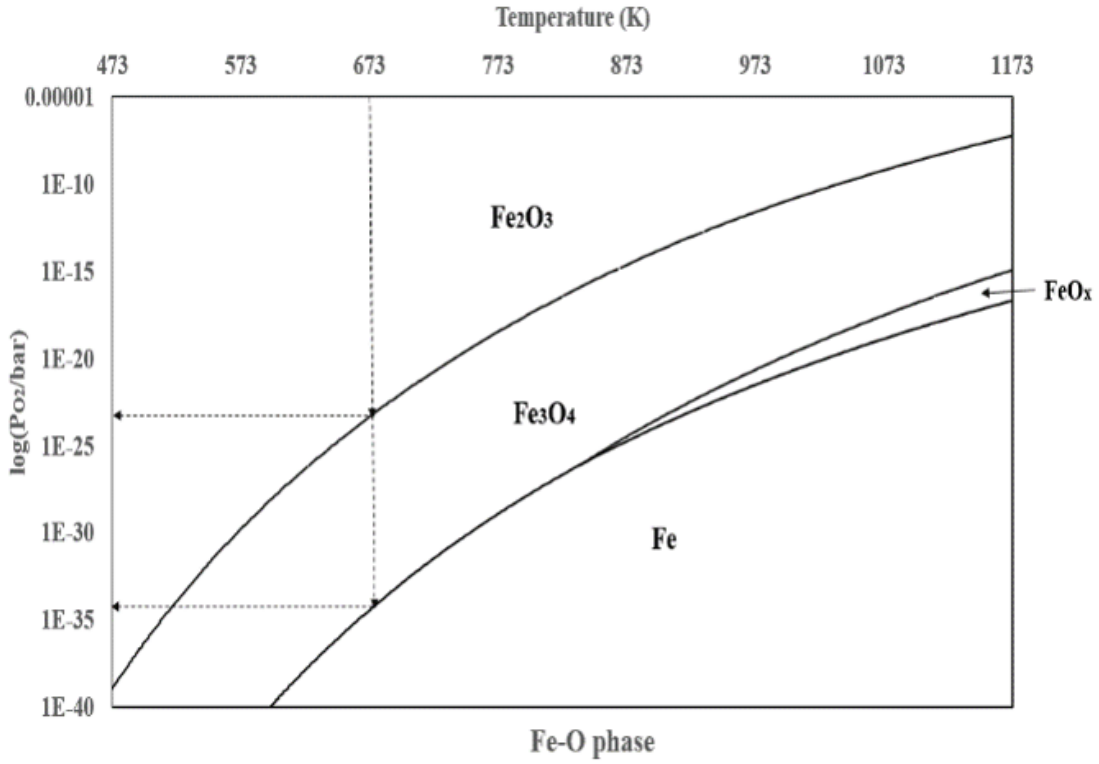

Fig. S5

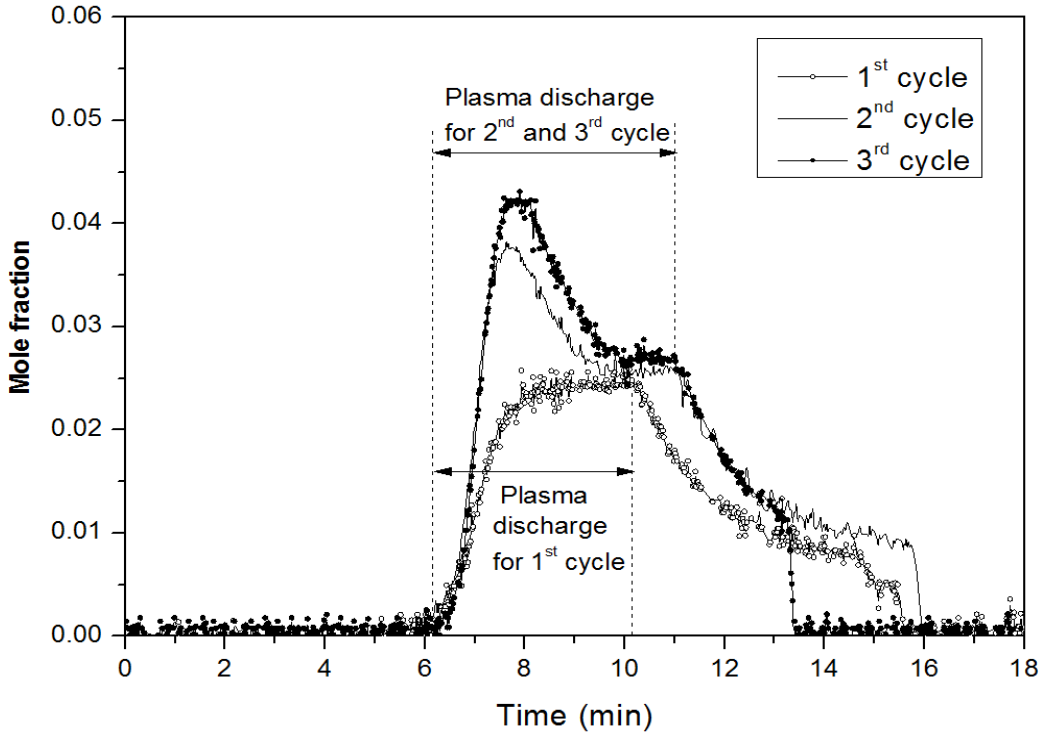

Table S1

Component	Fe_2O_3	Fe_3O_4	NiO	Ni	$NiFe_2O_4$	(Ni, Fe)	$NiAl_2O_4$
Collection Code from ICSD	15840	30860	9866	260169	40040	56386	9556

Table S2

Element	**Weight in wt%**	**σ in wt%**
C	6.59	0.06
O	10.84	0.03
Fe	20.28	0.05
Ni	62.2	0.07

Eq. S1

The energy cost in this manuscript was defined as:

$$\text{Energy cost} = \frac{(\frac{W}{B_{CH_4}\cdot\eta}+n_{CH_4})\cdot HHV_{CH_4}}{n_{H_2}},$$

where W is the applied plasma power, n_{H_2} is the amount of H_2 produced over processing time. B_{CH_4} is the chemical exergy of CH_4, which is ~ 52 MJ/kg. η is the efficiency from thermal to electricity energy and a value of 60% is assumed here. n_{CH_4} is the converted amount of CH_4, and HHV_{CH_4} is the high heating value of CH_4 (~ 55.5 MJ/kg).